Supplementary Information for: The Effect of Caesium Alloying on Ultrafast Structural Dynamics in Hybrid Organic-Inorganic Halide Perovskites

Nathaniel P. Gallop[1], Junzhi Ye[2,3], Greg Greetham[4], Thomas L.C. Jansen[5], Linjie Dai[2], Szymon J. Zelewski[2,6], Rakesh Arul[2], Jeremy J Baumberg[2], Robert Hoye[3], Artem A. Bakulin[1]

[1]Dept. of Chemistry – Imperial College London, Molecular Sciences Research Hub, 83 Wood Lane, London W12 0BZ
[2] Cavendish Laboratory, University of Cambridge, JJ Thomson Avenue, Cambridge CB3 0HE, United Kingdom
[3]Dept. of Materials – Imperial College London, Royal School of Mines, London SW7 2AZ
[4]Central Laser Facility, Rutherford Appleton Laboratory, Harwell Campus, Didcot, OX11 0QX
[5]Theoretical Chemistry, Materials Science Centre, Rijksuniversiteit Groningen (RuG), Nijenborgh 4, 9747 AG Groningen, The Netherlands
[6]Department of Semiconductor Materials Engineering, Faculty of Fundamental Problems of Technology, Wrocław University of Science and Technology, Wybrzeże Wyspiańskiego 27, 50-370 Wrocław, Poland

Contents

1. Optical Characterisation

1.1 Methods

1.1.1 X-Ray Diffraction

The crystalline structure of the perovskite films was investigated with an X-ray diffractometer (Bruker D8 Advance powder X-ray diffractometer) equipped with a Cu-Kα X-ray tube, using quartz/perovskite as samples measured with an air-free sample holder.

1.1.2 Time-Correlated Single Photon Counting (TCSPC)

TCSPC measurements were obtained by exciting the perovskite films with a Pico Quant LDH407 laser diode at 407 nm with a repetition rate of 0.1 MHz at different fluences. The emission signal was selected with a monochromator to obtain the desired emission wavelength and detected by a Hamamatsu R3809U-50 photomultiplier detector. Color long pass filters were utilized to remove the scattered photons from the excitation laser.

We fit the TCSPC data with a bi-exponential model given by:

$$y = y_0 + A_1 e^{-(x-x_0)/t_1} + A_2 e^{-(x-x_0)/t_2} \quad \text{(S1)}$$

We convolute this fitting model with a Gaussian ($\sigma \sim 1.41\ ns$) instrument response function. The resulting values obtained from fitting the decay curves in Fig. 2(c) (main text) are given in Table S1, below. In all cases the lifetime fitting error was approximately ±0.5—1 ns; as such, the values for t1 and t2 reported below are rounded to the nearest ns.

The average lifetime is obtained from the amplitude-weighted[1,2] average of the time components given in Table S1 using the formula:

$$\tau_{average} = \sum_n A_n \tau_n \Big/ \sum_n A_n \quad \text{(S2)}$$

The values for τ_{avg} given in Fig. 2(e) are likewise reported to the nearest nanosecond

Table S1 Fitted TCSPC lifetimes

Cs Content %	$\tau_{average}$ (ns)	t_1 (ns)	A_1	t_2 (ns)	A_2
0	5.95	6	2898	1131	253
10	8.16	7	1191	2156	107
20	6.81	7	2057	1015	240
30	4.01	4	10601	360	91

1.1.3 Photoluminescence Quantum Yield (PLQY)

The PLQY of the perovskite film was measured using a commercial setup from Ocean Optics with excitation from a 405 nm wavelength continuous wave (CW) diode laser.

1.2 Photoluminescence Spectra of $MA_{1-x}Cs_xPbI_3$

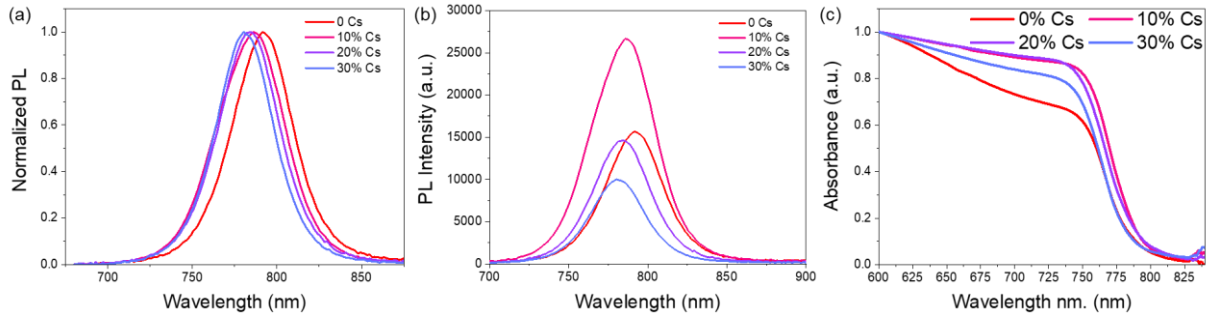

Figure S1 Photoluminescence. (a) Normalized PL spectra and (b) Un-normalized PL spectra of $Cs_xMA_{1-x}PbI_3$ (x=0-30%) thin films. (c) UV-Vis absorption spectra of $Cs_xMA_{1-x}PbI_3$ (x=0-30%) thin films.

1.2.1 PDS Fitting

The Urbach energy of the $Cs_xMA_{1-x}PbI_3$ thin films can be calculated by equation (S1).

$$\alpha(E) = \alpha_0 e^{\frac{E}{E_u}} \quad \text{(S1)}$$

where α is the absorption coefficient, E is the energy of the light absorbed, and E_u the Urbach energy.

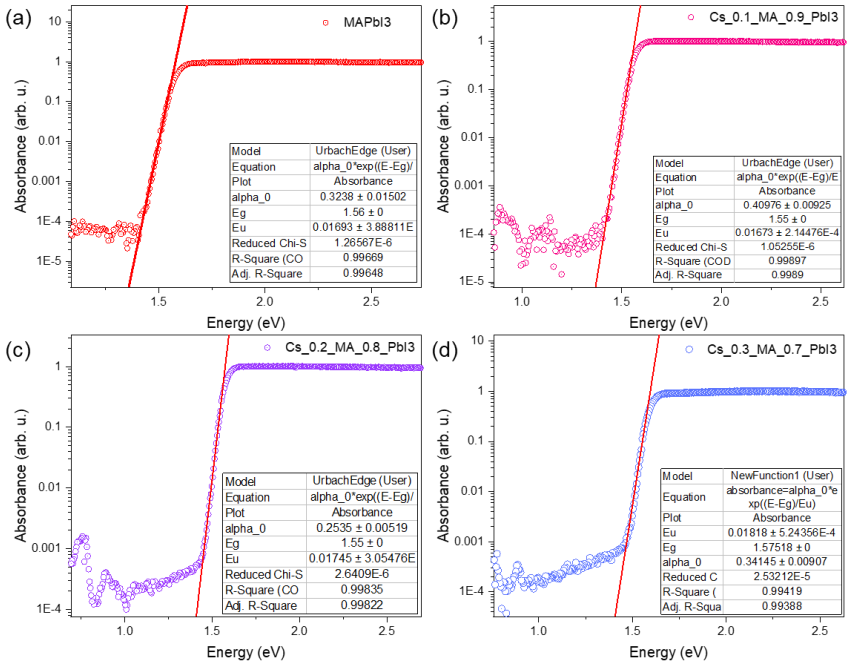

Figure S2 Urbach Energy and Bandgap fitting from PDS measurements. (a) For pure $MAPbI_3$ (b) For $Cs_{0.1}MA_{0.9}PbI_3$ (c) For $Cs_{0.2}MA_{0.8}PbI_3$ (d) For $Cs_{0.3}MA_{0.7}PbI_3$

Table S2 Summary of the optical properties.

Cs Content (%)	Avg. PL Lifetime (ns)	PLQY (%)	Urbach Energy (meV)	Bandgap (PDS) (eV)	Bandgap (UV-Vis) (eV)
0	5	0.303	16.93	1.567	1.590
10	8	0.433	16.73	1.548	1.566
20	7	0.270	17.45	1.555	1.572
30	4	0.206	18.18	1.575	1.582

2. Raman Spectra of $MA_{1-x}Cs_xPbI_3$

2.1 Methods

Raman spectroscopy measurements were performed with a Renishaw InVia microscope with a 100X objective, 0.9 N.A., with a 785 nm excitation laser (0.1 mW incident power), 1200 l/mm grating, and 1s integration time. Maps were collected by scanning the stage in the lateral directions while acquiring a Raman spectrum at each location. Each spectrum was then fitted with a quadratic sloping background and Gaussian peaks for each of the broad low-frequency bands.

2.2 Peak Analysis

Table S3. Summarized Raman peak fitting, including peak position and peak full width half maximum (FWHM).

Cs Content	0% Cs (cm^{-1})	10% Cs (cm^{-1})	30% Cs (cm^{-1})
Average Raman Peak Position (Peak 1)	151.89±1.92	151.31±0.64	147.85±3.10
Average Raman Peak Position (Peak 2)	217.33±4.24	218.47±6.65	221.79±8.62
Average Raman Peak FWHM (Peak 1)	43.08±3.67	49.40±3.71	55.15±8.66
Average Raman Peak FWHM (Peak 2)	76.20±21.61	51.39±8.58	65.05±51.10

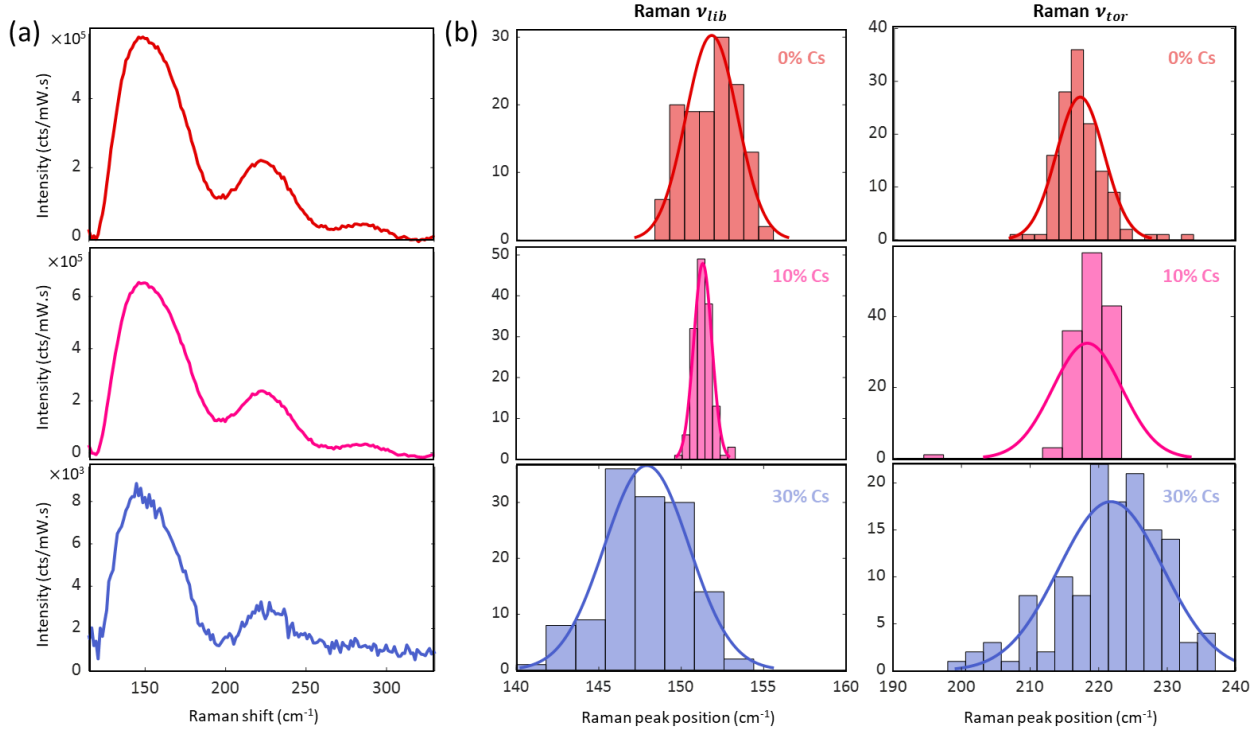

Figure S3. Raman Spectroscopy. (a) Raman Spectra of $MAPbI_3$, $Cs_{0.1}MA_{0.9}PbI_3$ and $Cs_{0.3}MA_{0.7}PbI_3$ thin films. (b) Fitted peak position for ν_{lib} and ν_{tor} in the Raman spectra for different Cs and MA ratio.

3. 2DIR Spectroscopy

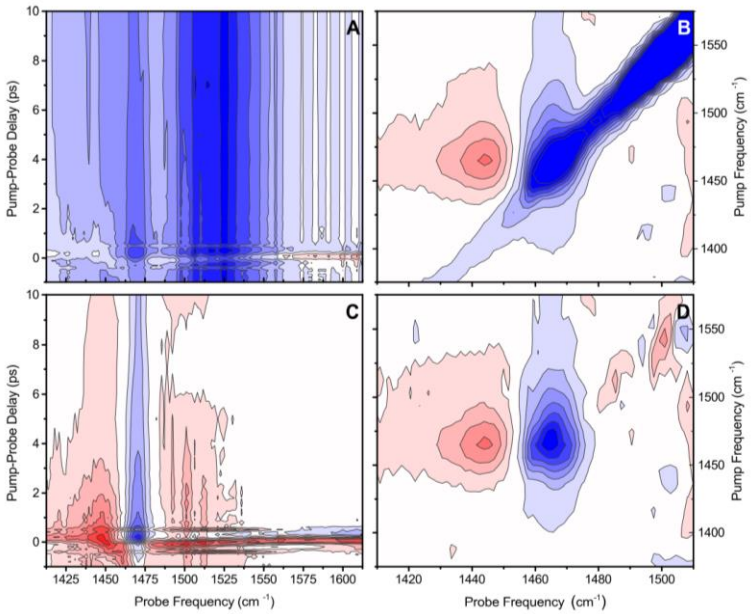

Figure S4. Examples of scattering effects in TRIR and 2DIR spectra. (A,C) TRIR map of $MAPbI_3$ without (A), with (C) scattering effects corrected, and (B,D) 2DIR maps of $MA_{0.8}Cs_{0.2}PbI_3$ without (B), and with (D) scattering effects corrected.

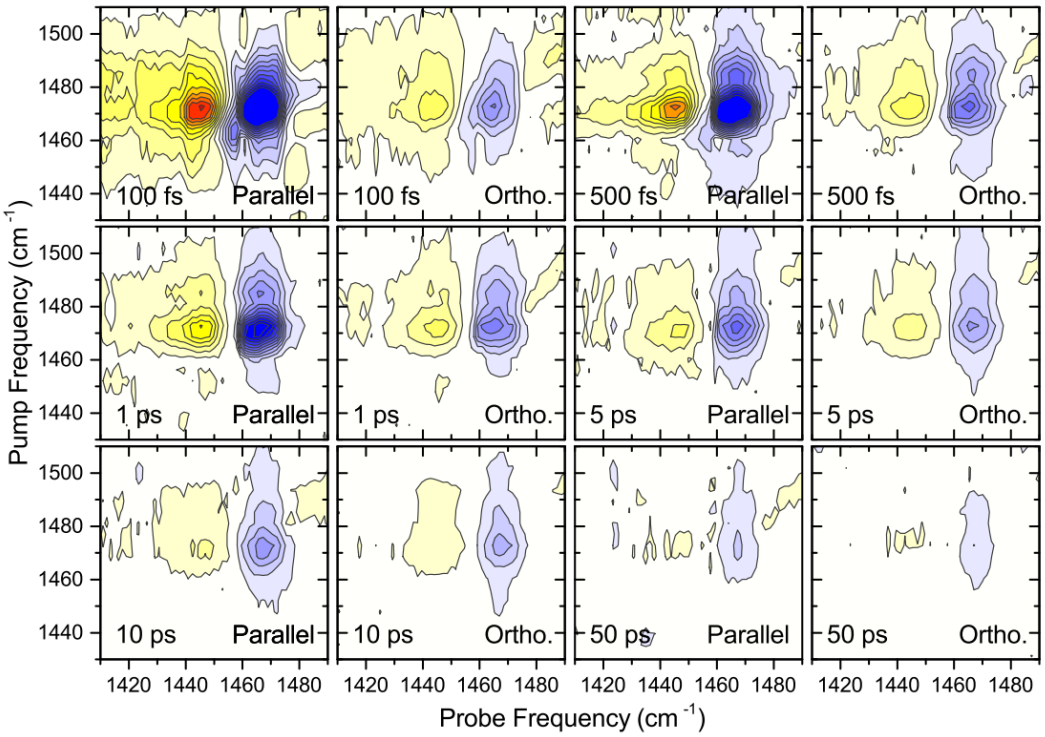

Figure S5. Evolution of the 2DIR spectra of $MA_{0.7}Cs_{0.3}PbI_3$ over increasing population times, utilizing probe pulses that are either parallel or orthogonal to the pump pulse

4. Computational Methods

The molecular dynamics simulations were performed with GROMACS 4.6.7 (SoftwareX, 2015, 1-2, 19-25). The systems were prepared with 216 Pb ions, 648 I ions, 194 MA ions, and 22 Cs ions. The Cs ions were placed completely randomly on the A-sites of the perovskite sites and a MA ion was placed on all other A-sites. The polarizable force field for the ions was previously described in[3] while the OPLS-AA force field was used for the organic ions[4]. As described in the main paper two simulations were performed with either isotropic or anisotropic pressure coupling with the Parrinello-Rahman barostat[5] with a 10 ps coupling timescale. The V-rescale thermostat with a 1 ps timescale. A 1.4 nm cut-off was used for short-range interactions and long-range interactions were described using the Particle-Mesh-Ewald sum[6]. The simulations were performed for 1 ns after equilibration for both systems. The simulation timesteps were 0.5 fs. For the anisotropic simulations the box dimensions were on average 3.660, 3.653, 3.759 nm demonstrating symmetry breaking very similar to that observed in experiments, while the isotropic simulation gave an average box side length of 3.69 nm in all direction.

References

(1) Zatryb, G.; Klak, M. M. On the Choice of Proper Average Lifetime Formula for an Ensemble of Emitters Showing Non-Single Exponential Photoluminescence Decay. *J. Phys. Condens. Matter* **2020**, *32* (41), 11. https://doi.org/10.1088/1361-648X/ab9bcc.

(2) Sillen, A.; Engelborghs, Y. The Correct Use of “Average” Fluorescence Parameters. *Photochem. Photobiol.* **1998**, *67* (5), 475–486. https://doi.org/10.1111/j.1751-1097.1998.tb09082.x.

(3) Gallop, N. P.; Selig, O.; Giubertoni, G.; Bakker, H. J.; Rezus, Y. L. A.; Frost, J. M.; Jansen, T. L. C.; Lovrincic, R.; Bakulin, A. A. Rotational Cation Dynamics in Metal Halide Perovskites: Effect on Phonons and Material Properties. *J. Phys. Chem. Lett.* **2018**, *9* (20), 5987–5997. https://doi.org/10.1021/acs.jpclett.8b02227.

(4) Jorgensen, W. L.; Tirado-Rives, J. The OPLS Potential Functions for Proteins. Energy Minimizations for Crystals of Cyclic Peptides and Crambin. *J. Am. Chem. Soc.* **1988**, *110* (6), 1657–1666. https://doi.org/10.1021/ja00214a001.

(5) Parrinello, M.; Rahman, A. Crystal Structure and Pair Potentials: A Molecular-Dynamics Study. *Phys. Rev. Lett.* **1980**, *45* (14), 1196–1199. https://doi.org/10.1103/PhysRevLett.45.1196.

(6) Essmann, U.; Perera, L.; Berkowitz, M. L.; Darden, T.; Lee, H.; Pedersen, L. G. A Smooth Particle Mesh Ewald Method. *J. Chem. Phys.* **1995**, *103* (19), 8577–8593. https://doi.org/10.1063/1.470117.